Biomaterials 34 (2013) 598–605

Contents lists available at SciVerse ScienceDirect

Biomaterials

journal homepage: www.elsevier.com/locate/biomaterials

# Tumor suppression via paclitaxel-loaded drug carriers that target inflammation marker upregulated in tumor vasculature and macrophages

Spencer Park [a], Sungkwon Kang [a], Xiaoyue Chen [a], Esther J. Kim [a], Jeeyoung Kim [a], Nahae Kim [b], Juyoung Kim [b], Moonsoo M. Jin [a,c,*]

[a] Department of Biomedical Engineering, Cornell University, Ithaca, NY 14853, USA
[b] Department of Advanced Materials Engineering, Kangwon National University, Samcheok 245-711, South Korea
[c] Department of Radiology, Weill Cornell Medical College, New York, NY 10065, USA

ARTICLE INFO

*Article history:*
Received 14 July 2012
Accepted 3 October 2012
Available online 23 October 2012

*Keywords:*
Inflammation
Cancer
Nanoparticle
Targeted drug delivery
ICAM-1

ABSTRACT

Clinically approved chemotherapeutic nanoparticles may provide advantages over free drugs by achieving slower clearance and preferential accumulation in tumors. However, the lack of leaky vasculatures can create barriers to the permeation of ~100 nm-sized nanoparticles in solid tumors. We hypothesized that nanoparticles designed to target both tumor and tumor stroma would penetrate deeper into the tumors. To construct such comprehensive drug carriers, we utilized cross-linked amphiphilic polymer nanoparticles and functionalized them to target ICAM-1, a biomarker prevalent in various tumors and inflamed tumor stroma. The targeting moiety was derived from the modular domain present in $\alpha_L$ integrin, which was engineered for high affinity and cross-reactivity with human and murine ICAM-1. ICAM-1-selective delivery of paclitaxel produced potent tumor suppression of not only ICAM-1-positive cervical cancer cells but also ICAM-1-negative tumors, presumably by causing cytotoxicity in tumor-associated endothelium ($CD31^+$) and macrophages ($CD68^+$) over-expressing ICAM-1. Contrary to the strategies of targeting only the tumor or specific tumor stromal constituents, we present a strategy in delivering therapeutics to the major cellular components of solid tumors. Drug carriers against inflammation-biomarkers may be effective against many different types of tumors, while being less susceptible to the highly mutable nature of tumor markers.



## 1. Introduction

Achieving site-specific delivery of drug carriers, while minimizing unwanted distribution, has been one of the pursued goals in cancer therapy. Current drug carriers of ~100 nm in size can be selectively delivered into tumors through the enhanced permeability and retention (EPR) effect [1]. Several different nanoparticles employing the EPR effect have been approved for clinical use, e.g., Doxil and Abraxane. Tumor killing by non-molecularly targeted carriers may be accomplished via slow release of drugs within the tumor interstitial space or from the release of drugs inside cells after non-specific uptake [2]. However, current drug delivery systems fall short on achieving adequate concentrations of drugs in tumor cells in hypoxic regions as well as in malignancies that lack leaky vasculature, promoting the development of drug-resistance [3]. Much of the limitations of non-targeted nanoparticle-based drug carriers come from the fact that (i) leaky pores in tumor vessels are often sparsely distributed and some tumors completely lack well-perfused vasculatures, leading to heterogenous or limited dissemination of nanoparticles [1,4], (ii) increased interstitial pressure within tumors tends to rapidly clear nanoparticles distributed outside of cells, and (iii) surface modifications of drug carriers to reduce non-specific uptake by phagocytic cells and opsonization also disfavor the uptake of nanoparticles by tumors [2,5,6].

To overcome such physiological barriers, local applications of hyperthermia [7], photosensitization [8], and ultrasound [9] have been used to increase the permeability of tumor vessels and thus, the penetration of drug carriers throughout the tumor. Alternatively, new types of nanoparticles to address the aforementioned problems have also been engineered. For example, drug carriers possessing the ability to target tumor stromal constituents, including the vasculature [10,11] and/or tumor-associated macrophages [12], have shown promising results. Similarly, we have previously found that a molecule called intercellular adhesion molecule (ICAM)-1 was highly induced in endothelial cells within

* Corresponding author. Department of Radiology, Weill Cornell Medical College, New York, NY 10065, USA.
*E-mail address:* moj2005@med.cornell.edu (M.M. Jin).

0142-9612/$ – see front matter © 2012 Elsevier Ltd. All rights reserved.
http://dx.doi.org/10.1016/j.biomaterials.2012.10.004

and in the vicinity of tumors [13]. ICAM-1 is a cell adhesion molecule normally expressed at low levels in a variety of cell types but over-expressed in inflammation and neoplastic conditions, likely due to the activation of the transcriptional factor, NF-κB. ICAM-1 is upregulated in many carcinomas including breast, colon, non-small cell lung, and gastric tumors [16–21], where the over-expression of ICAM-1 is correlated with tumor progression, metastatic capability, and poor prognosis [22–24]. Upregulation of ICAM-1 within the tumor stroma is, therefore, consistent with the increasing reports on the implication of inflammation in tumor initiation, progression, and metastasis [14,15]. More importantly, it can be speculated that drug carriers designed to target ICAM-1 would be broadly effective in eradicating not only carcinoma cells expressing ICAM-1 but also those lacking ICAM-1 by killing the tumor stromal cells that are critical to tumor growth and metastasis. The delivery of drugs against multi-cellular components comprising tumors may also be less susceptible to the development of drug-resistance.

In order to create ICAM-1-specific drug carriers, we used a modular domain called the inserted (I) domain derived from the integrin, leukocyte function associated antigen-1 (LFA-1; also known as $\alpha_L\beta_2$ or CD11a/CD18), where the I domain is the only region that provides molecular contact with ICAM-1. The I domain in its native sequence, separated from LFA-1, exhibits a low level of binding to ICAM-1, and was therefore engineered for high affinity and cross-reactivity with human and murine ICAM-1 [25–27]. LFA-1 I domain's reaction with murine ICAM-1 is an important property that permits selectivity studies of drug carriers against both the ICAM-1-expressing human tumors and the inflamed murine tumor microenvironment in mouse models of human cancer. At the same time, this feature enables us to analyze the unintended delivery to the low, yet widespread, expression of ICAM-1 in many different cellular types. As a drug carrier, we employed nanoparticles synthesized with cross-linked amphiphilic copolymer, providing a hydrophobic core for encapsulation of hydrophobic molecules and hydrophilic corona for stability in vivo as well as facile conjugation with targeting moieties [28]. Drug carriers designed to target markers prevalent in carcinomas and inflamed tumor microenvironment may prove effective against many different types of cancers.

## 2. Materials and methods

### 2.1. Production of high-affinity LFA-1 I domain

Recombinant LFA-1 I domain with a His-tag at the N-terminal was produced in BL21(DE3) *Escherichia coli* cells (Invitrogen) as described previously [26]. Briefly, after protein induction with 1 mM IPTG (isopropyl-β-D-thiogalactoside), *E. coli* cells were resuspended in 10 ml of the washing buffer (50 mM Tris (pH 8.0), 23% w/v sucrose, 0.5% w/v Triton X-100, 1 mM ethylenediaminetetraacetic acid (EDTA)), sonicated, and centrifuged again to purify the inclusion body. The inclusion bodies were solubilized with 20 ml of the solubilization buffer (50 mM Tris (pH 8.0), 6 M Guanidine-HCl) for 1.5 h at 4 °C with stirring, after which the solution was diluted with 2 l of refolding buffer (50 mM Tris (pH 8.0), 10% glycerol, 1 mM $MgCl_2$) and stirred slowly at 4 °C overnight for the refolding process. Finally, the protein was concentrated down to 1–5 ml (Amicon 3 kDa MWCO Millipore), filtered through a 0.45 μm filter (Nalgene), and purified by gel filtration chromatography (Superdex-75, GE Healthcare Life Sciences ÄKTApurifier™).

### 2.2. Preparation of I domain-coated urethane acrylate nonionomer (UAN) nanoplatforms

The synthesis of cross-linked UAN bound to nickel-nitriloacetic acid (NTA-UAN) was previously described [28]. In brief, UAN consists of 1:3:2:1 molar ratio of glycerol propoxylate:toluene diisocyanate:2-hydroxyethyl methacrylate (HEMA):-polyethylene glycol (PEG). 50 mg of the UAN monomers were cross-linked by the reaction between the vinyl groups of HEMA in 10 ml of dimethyl sulfoxide (DMSO, Sigma Aldrich) at 65 °C overnight with vigorous stirring, catalyzed by 2 mg of azobisisobutyronitrile (AIBN, Sigma Aldrich). The average molecular weight of the resulting UAN chains was 6700 Da (measured by mass spectrometer (MALDI Micro MX, Waters)) with a polydispersity of 2.0 (measured via ambient temperature gel permeation chromatography (GPC, Waters)). To incorporate the NTA moiety on the hydroxyl end of the PEG groups in polymerized UAN, 10 mg of $N_\alpha$,$N_\alpha$-Bis(carboxymethyl)-L-lysine hydrate (NTA analog, Sigma Aldrich) in 0.1 ml DMSO was mixed with 6.4 mg of TDI (molar ratio of NTA to TDI was 1:1) for 2.5 h at room temperature to prepare NCO-terminated NTA-TDI complexes. Then the NTA-TDI solution was added to 5 ml of DMSO containing 50 mg of cross-linked UAN and mixed overnight at room temperature to covalently link NCO of NTA-TDI to OH groups of UAN chains. In order to form nanoparticles, the cross-linked UAN chains dissolved in DMSO were diluted in HEPES buffer saline (HBS) at a volume ratio of 1:100 (DMSO:HBS).

Previously, the size distribution (hydrodynamic radius) of NTA-UAN formulations encapsulating various hydrophobic agents was determined to be ~45–60 nm using dynamic light scattering (Malvern Instruments) [28]. In addition, transmission electron microscopy images revealed that bare UAN nanoparticles were spherical, uniformly sized, and well dispersed [28]. The payloads such as DiO (Invitrogen), DiR (Invitrogen), and Paclitaxel (PTX) (Sigma) were added to UAN chains in DMSO at 0–20% of UAN weight prior to dilution with HBS. The NTA moiety of UAN was charged with 10 mM $NiCl_2$ for 30 min at RT. Excess payloads, $NiCl_2$, and DMSO were removed via dialysis and subsequent concentration of the solution down to appropriate volume. Ni-NTA-UAN was then incubated with I domain at a weight ratio of 25:1 (Ni-NTA-UAN:I domain) at 4 °C for 30 min to form I domain-coated cross-linked UAN (Id-UAN) before being used in subsequent experiments.

### 2.3. $EC_{50}$ analyses

HeLa cells cultured in a 24-well plate were treated with 300 μl of the labeling buffer (pH 7.4 PBS, 1% (w/v) BSA, 1 mM $MgCl_2$) containing varying concentrations of UAN(PTX) (non-targeted cross-linked UAN carrying PTX), Id-UAN(PTX) (I domain-bound UAN(PTX)), or PTX. The amount of PTX ranged from 0.1% to 17% of UAN (w/w). Ten minutes after the treatment, cells were washed twice with the labeling buffer and resuspended in 300 μl of the culture media without FBS for 72 h. Cell viability was then measured by directly counting cells on a hemocytometer. Cells labeled with trypan blue were excluded in cell counting.

### 2.4. Developing subcutaneous lipopolysaccharde (LPS) mouse model

100 μl of LPS (1 mg/ml in PBS) and PBS were bilaterally injected into the lower flanks of 7-week-old female severe combined immunodeficiency (SCID) mice. All animal experiments were conducted in compliance with the regulations defined by the Institutional Laboratory Animal Use and Care Committee of Cornell University.

### 2.5. Developing subcutaneous tumor xenograft mouse model

$3 \times 10^6$ human cervical cancer HeLa cells and human embryonic kidney 293T cells mixed with Matrigel (BD) in equal volume (150 μl each) were injected bilaterally into front lower flank areas of 7-week-old female SCID mice. Once the tumor size reached approximately 100 $mm^3$ (7–10 days), mice were used for subsequent treatments.

### 2.6. Near-IR optical imaging of mice

Ex vivo imaging was performed 18–24 h after retro-orbital injection of UAN(-DiR) or Id-UAN(DiR) using an NIR camera (Luca, Andor Technology). Each injection consisted of 200 μg of UAN. Image analysis was performed using Matlab R2007a (MathWorks) and ImageJ (NIH).

### 2.7. Tumor cytotoxicity assay

Mice were randomized into three groups ($n = 10$ each) for the following treatments given every 3 days for a total of three interventions: retro-orbital intravenous (i.v.) injection of HBS as a control, i.v. injection of 200 μg (UAN weight) of UAN(PTX), or i.v. injection of 200 μg (UAN weight) of Id-UAN(PTX). Tumor size was measured daily, while the blood collection from tail-vein (~200 μl) and body weight measurement for the toxicity assays were carried out on the days of injection.

### 2.8. Liver toxicity assay

Blood samples from tail-vein collected in capillary tubes were snap-frozen in liquid nitrogen and kept at −80 °C until being analyzed for the activity levels of aspartate transaminase (AST) and alanine transaminase (ALT) according to the manufacturer's protocol (BioVision).

### 2.9. Flow cytometry and immunofluorescence analysis of ex vivo tissues

Tissues from tumors and other organs were collected from tumor bearing mice with or without in vivo injections of Id-UAN(DiO) or UAN(DiO). Harvested tissues were diced and digested with collagenase A (1 mg/ml) for 8 h before being strained. Collected cells were washed once with labeling buffer and incubated for 30 min

using rat anti-mouse CD31 monoclonal antibody (mAb) (MEC13.3, BD), rat anti-mouse CD68 mAb (FA-11, BioLegend), rabbit anti-murine ICAM-1 polyclonal antibody (M-19, SantaCruz), rabbit anti-human ICAM-1 mAb (LB-2, SantaCruz). After labeling with primary antibodies, cells were washed with labeling buffer and incubated with anti-rat or anti-rabbit phycoerythrin (PE)-labeled secondary antibodies (Invitrogen). Subsequently, flow cytometry experiment was carried out to measure the fluorescence intensity of DiO as well as the antibodies (Beckman Coulter EPICS XL-MC). The data were analyzed using FlowJo (Tree Star).

### 2.10. Statistical analysis

Data were expressed as mean ± standard deviation of at least triplicate samples. Two-way ANOVA and Bonferroni post hoc test were carried out in order to assess which groups significantly differed from others. All of the statistical analyses were performed using GraphPad Prism 5 (Graphpad Software).

## 3. Results

### 3.1. Biodistribution, selectivity, and toxicity of drug carriers

Prior to testing the efficacy of ICAM-1-specific nanoparticles in eradicating tumors, we first evaluated their biodistribution, selectivity to ICAM-1, and toxicity with or without surface conjugation with I domain. The engineered I domain we utilized in this study contains F265S/F292G mutations and binds human and murine ICAM-1 with high affinity (2–6 nM $K_D$) [29]. Cross-linked UAN nanoparticles contain a core formed by polypropylene oxide networks, which can retain hydrophobic molecules at up to 20% w/w of UAN, and exhibit slower release kinetics with increasing hydrophobicity of payloads [28]. Almost irreversible retention of water-insoluble near-infrared dye, DiR, by cross-linked UAN suspended in an aqueous solution was exemplified by negligible partitioning of DiR into chloroform, while free DiR was almost entirely dissolved in chloroform (Fig. 1A).

Biodistribution of UAN(DiR) or Id-UAN(DiR) into the major organs and the sites of interest was quantified by near-infrared imaging of organs ex vivo. Two different mouse models were chosen to examine the difference in biodistribution caused by the presence of I domain on UAN: (1) untreated mice to assess the targeting of basal expression of ICAM-1 and (2) mice with subcutaneous injection of lipopolysaccharide (LPS) to examine the ability of Id-UAN to localize to the site of ICAM-1 over-expression. Major organs and the subcutaneous treatment sites were harvested 18 h post-injection of UAN particles for biodistribution analysis. In untreated mice, irrespective of the conjugation with I domain, liver and spleen accounted for 66% of UAN nanoparticles that accumulated into major organs (Fig. 1B). Although at much lower levels, Id-UAN(DiR) showed a higher level of accumulation than UAN(DiR) in lungs and kidneys. Next, using a mouse model with subcutaneous bilateral injections of LPS and PBS (12 h), we examined the influence of localized induction of ICAM-1 on nanoparticle distribution (Fig. 1C). Notably, the presence of I domain on the surface of UAN caused a 3-fold higher concentration at the LPS injection site compared to the PBS injection site. In contrast to Id-UAN(DiR), UAN(DiR) accumulated significantly less into both LPS and PBS sites, displaying insignificant difference between the two regions. Although the overall pattern of biodistribution into the major organs in LPS mouse model was comparable to that of the untreated mice, the higher level of uptake was observed in the liver and spleen, likely caused by the LPS seeping into circulation and triggering a mild systemic inflammation. This would then enhance the phagocytic activity of immune cells and dilate the vessels, resulting in elevated accumulation into some of the major organs.

The high accumulation of the particles in the liver, however, raised a concern for possible systemic side effects. We carried out a liver toxicity assay by measuring the serum activity levels of aspartate transaminase (AST) and alanine transaminase (ALT), two enzymes that often serve as markers for liver damage (Fig. 1D). AST and ALT levels measured between 0 and 48 h after LPS injection, used to artificially induce liver toxicity were gradually elevated, peaking at 24 h and dropping back to normal levels by 48 h. In contrast, ALT/AST levels after UAN(DiR) injection remained below the threshold for liver toxicity, and did not differ greatly from mice treated with PBS.

### 3.2. Tumor targeting: tissue- and cell-level distribution analysis

To confirm the selectivity of UAN conferred by the I domains toward ICAM-1 over-expressed in tumors or in inflamed tumor

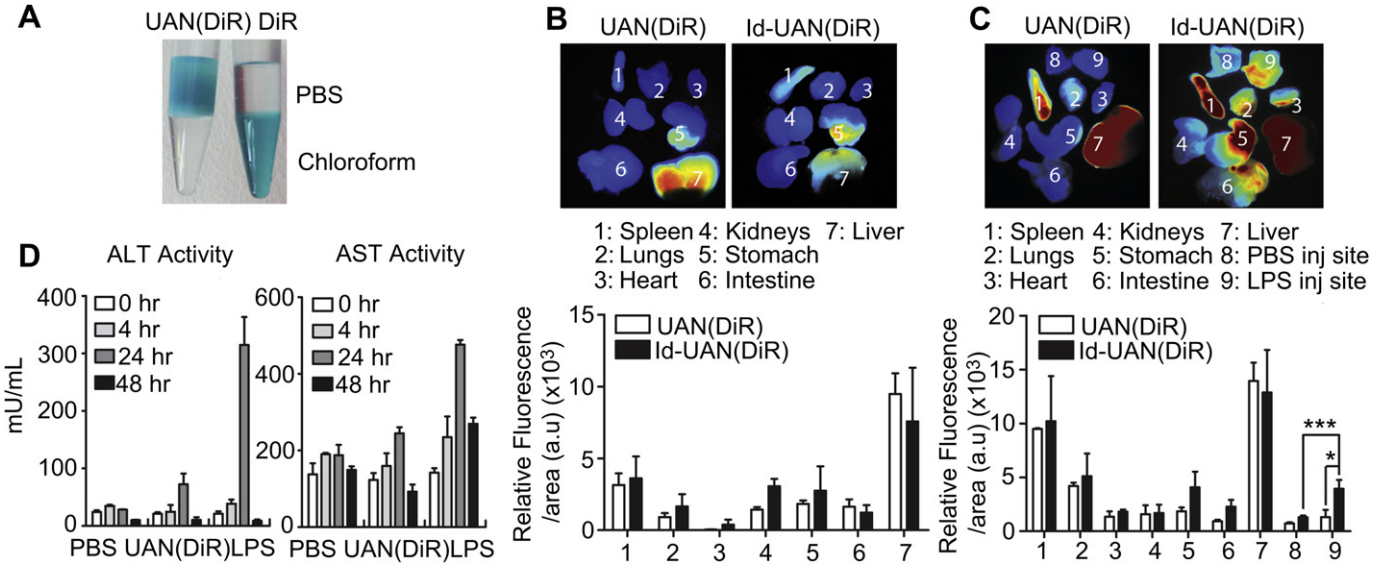


**Fig. 1.** Biodistribution, selectivity, and toxicity of drug carriers. (A) Partitioning of DiR from chloroform into the hydrophobic core of UAN dispersed in PBS. 0.05 mg of DiR was dissolved in 0.05 ml of DMSO or DMSO containing cross-linked UAN (1 mg) before being added to a liquid bilayer of PBS/chloroform (0.5 ml each) and shaken gently for 4 h. (B) NIR imaging and quantification of UAN(DiR) and Id-UAN(DiR) dispersed throughout the major organs after intravenous injection at 24 h post-injection ($n = 6$; a.u. = arbitrary unit). (C) UAN(DiR) and Id-UAN(DiR) distribution at 24 h post-injection in LPS mouse model. Nanoparticles were injected 12 h after subcutaneous LPS/PBS injection ($n = 4$). (D) Liver toxicity of UAN(DiR) compared to LPS and PBS. Bar graphs represent serum activity levels of ALT and AST ($n = 6$) (Error bars are standard deviations (SD) $^*p < 0.05$, $^{***}p < 0.001$; Two-way ANOVA test followed by Bonferroni post hoc test).

stroma, we used a mouse model harboring bilateral subcutaneous xenografts of ICAM-1-positive HeLa and ICAM-1-negative 293T tumors. When tumors grew to ~100 $mm^3$ in size, mice were intravenously injected with UAN nanoparticles and imaged at 24 h post-injection. Id-UAN(DiR) was found at both tumor sites, whose fluorescence levels were significantly higher than those in the tumors injected with UAN(DiR) (5.1-fold in HeLa and 2.1-fold in 293T tumor) (Fig. 2A). Furthermore, 2.9-fold increase in accumulation into HeLa over 293T was observed with Id-UAN(DiR), while comparable amounts were found in both tumors with UAN(DiR). We then examined if increased delivery of Id-UAN(DiR) into 293T tumor was from targeting of ICAM-1 induced in tumor stromal cells, such as vasculature endothelium and/or tumor-associated macrophages. To first confirm if 293T cells have induced ICAM-1 in the course of tumor growth, we carried out immunofluorescence flow cytometry on the cells isolated from untreated HeLa and 293T tumors (Fig. 2B). From labeling of cells with antibodies against human or murine ICAM-1 (CD54), we found only murine ICAM-1 was induced in 293T tumors while both human and murine ICAM-1 were present in HeLa tumors, proving the lack of ICAM-1 expression in 293T cells and upregulation of ICAM-1 in tumor stromal cells. Next, to test if $CD31^+$ and $CD68^+$ cells were the cellular types responsible for the presence of ICAM-1 in tumor stroma, we labeled the cells isolated from tumors with antibodies against ICAM-1 along with antibodies against either CD31 or CD68. Indeed, significantly higher percentage of tumor-associated $CD31^+$ and $CD68^+$ cells exhibited over-expression of ICAM-1, while corresponding cellular types derived from skin and spleen were

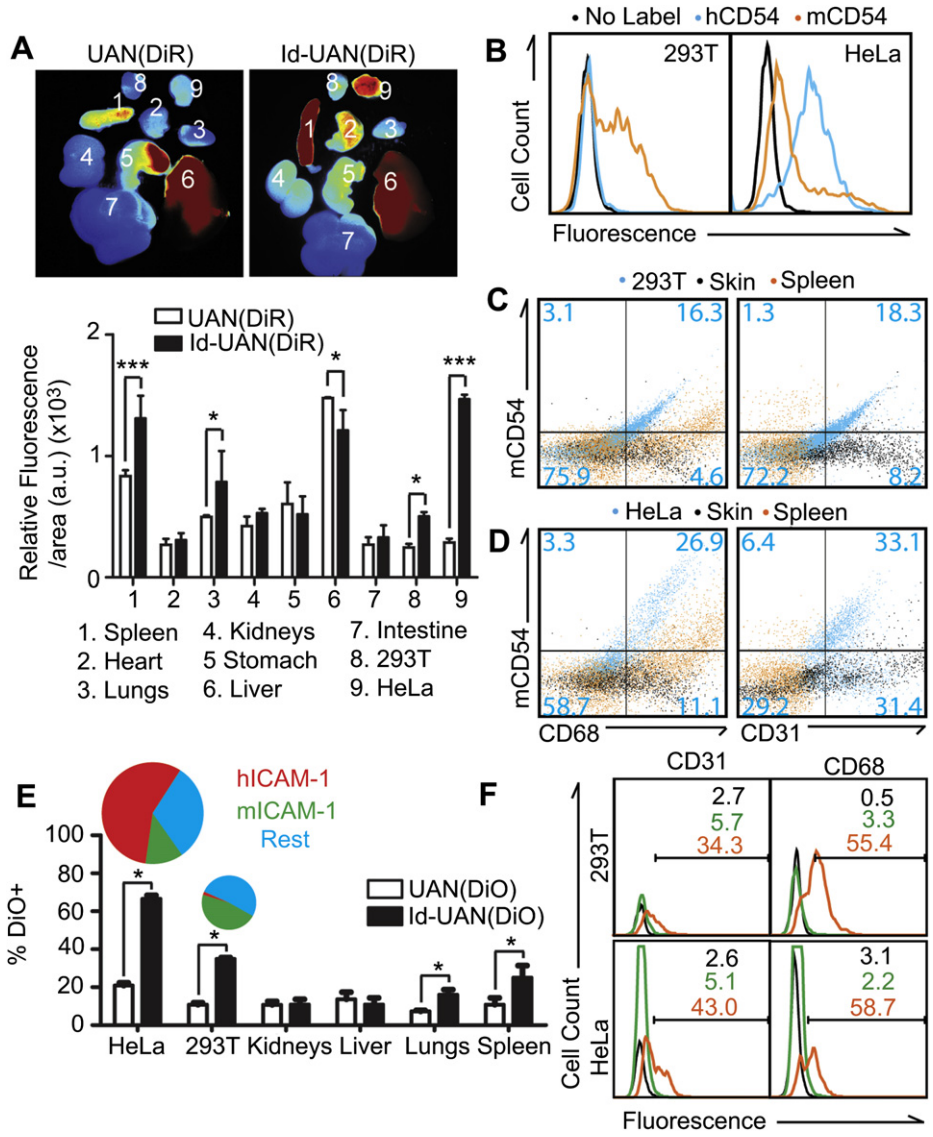


**Fig. 2.** Tumor targeting: tissue-/cell-level distribution analysis. (A) Major organs and tumors at 24 h post-injection of nanoparticles. Mice bearing bilateral HeLa and 293T tumors were injected with either UAN(DiR) or Id-UAN(DiR) ($n = 8$). (B) CD54 induction in tumor stroma. Cells isolated from untreated HeLa/293T tumors were labeled with antibodies against human (hCD54) or murine ICAM-1 (mCD54). (C and D) Cells isolated from tumors (C: 293T, D: HeLa), skin, and spleen were dual-labeled for mCD54 and mCD68/mCD31 to identify cellular types expressing mCD54. Numbers indicate the percentage of gated populations of cells isolated from tumors. (E) Differentiating cellular uptake of UAN particles from those trapped in an extracellular space. Fluorescence of isolated cells from tumors was measured using flow cytometry ($n = 4$). Specificity of Id-UAN(DiO) against ICAM-1 is shown in pie charts. After injection of Id-UAN(DiO) or UAN(DiO), cells from tumors were isolated and labeled with antibodies against hCD54 or mCD54. (F) Mice carrying bilateral HeLa and 293T tumors were intravenously injected with Id-UAN(DiO) (orange), UAN(DiO) (green), or PBS (black) 24 h preceding the excision and cell isolation. The cellular components of tumors labeled with Id-UAN(DiO) vs. UAN(DiO) were identified via labeling for mCD31, or mCD68 (Error bars are SDs. $^*p < 0.05$, $^{***}p < 0.001$; two-way ANOVA test followed by Bonferroni post hoc test.). (For interpretation of the references to color in this figure legend, the reader is referred to the web version of this article.)

mostly negative for ICAM-1 expression (CD31/CD68 from skin; CD31 from spleen) or induced at lower levels (CD68 from spleen) (Fig. 2C and D).

Tumor-targeting nanoparticles that have escaped from circulation through leaky vasculature would diffuse through the tumor interstitial space. Subsequent uptake of these particles is influenced by the intrinsic properties of particles (i.e., size, charge, shape) and the presence of active molecular targeting moieties. Therefore, some of the signals coming from the tumors and organs may be due to the particles being merely trapped in the extracellular or interstitial space. Since UAN nanoparticles are designed to deliver drugs directly into cells for effective cytotoxicity rather than through slow release within extracellular space, we carried out flow cytometry to quantify cellular uptake of UAN particles loaded with a hydrophobic green fluorescent dye, DiO (Fig. 2E). Similar to the tissue-level analysis, Id-UAN(DiO) was taken up by higher percentages of cells harvested from both tumors, with $DiO^+$ cells in HeLa tumor being 2.0-fold higher compared to the $DiO^+$ cells in 293T. Cellular uptake of Id-UAN nanoparticles in both tumors was specific to ICAM-1; 50–80% of DiO-positive cells were also positive for either human or murine ICAM-1 (Fig. 2E; shown in the pie charts). Cellular-level analysis, however, showed that larger amounts of nanoparticles were internalized by the tumors than the organs (e.g., liver and spleen) which is in contrast to the ex vivo imaging of the organs and tumors that showed higher levels in the organs. This discrepancy, therefore, should point to the possibility of the particles being present in the extracellular spaces of these organs, causing them to be removed during the process of isolating cells for flow cytometry.

In order to quantify the percentage of tumor stromal cells that had internalized Id-UAN(DiO) and UAN(DiO), HeLa and 293T tumors were excised and digested for another series of flow cytometry analyses, conducted at 24 h after the injection of Id-UAN(DiO) and UAN(DiO). Collected cells were labeled with antibodies against CD31 and CD68. We found that among DiO-positive cells that were analyzed, 35–60% of the cells were positive for CD31 or CD68, proving that Id-UAN(DiO) was indeed taken up by both the vasculature endothelium and macrophages, as the two major constituents in tumor stroma (Fig. 2F).

### 3.3. Greatly enhanced $EC_{50}$ via molecular interaction-guided drug delivery

In an attempt to validate UAN as an effective drug delivery vehicle, we used paclitaxel, a water-insoluble chemotherapeutic drug. After encapsulation of PTX, we first examined the effectiveness of Id-UAN(PTX) in specifically attenuating the growth of ICAM-1-expressing cells in vitro (Fig. 3A). HeLa cells were exposed to either free paclitaxel, UAN(PTX), or Id-UAN(PTX) for only 10 min to model the transient exposure of drugs to a tumor in an in vivo system. Cells were then cultured for 72 h prior to cell viability quantification. Compared to UAN(PTX), which would induce cell death through slow release of PTX or non-specific uptake, the attachment of the I domain to the particles drastically improved the cytotoxic effects ($EC_{50} = 1$ μM by Id-UAN(PTX) vs. 37.5 μM by UAN(PTX)), highlighting the added advantage of active targeting for drug carriers such as UAN. Free PTX resulted in $EC_{50} = 63$ μM, significantly higher than those reported in other studies with longer incubation times, indicating PTX was not efficiently taken up by the cells during the 10-min exposure. Possible cytotoxic effects induced by UAN particles themselves were also examined by treating the cells with only the carrier, Id-UAN, at different concentrations. The results demonstrated that empty vehicles on their own ($EC_{50} = 4.4$ mg/ml) would have minimal cell killing effect

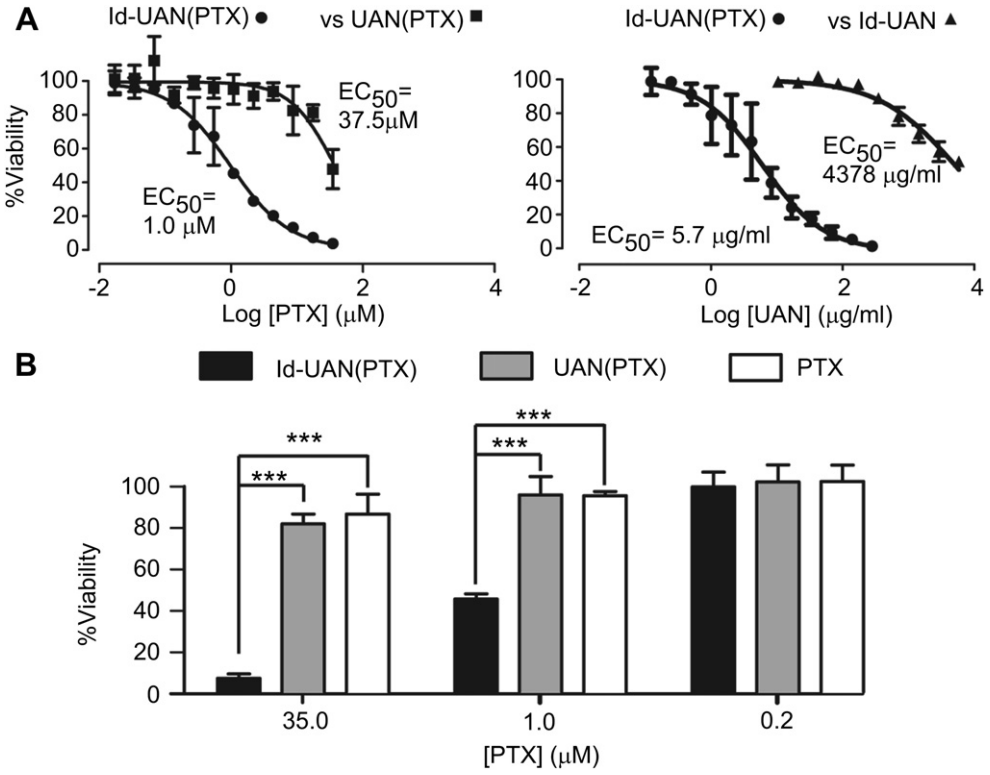


**Fig. 3.** In vitro $EC_{50}$ comparison between Id-UAN(PTX), UAN(PTX), and PTX. (A) HeLa cells subcultured in 24-well plates were treated for 10 min with varying concentrations of Id-UAN(PTX), UAN(PTX), PTX, or Id-UAN. At 72 h, cells were stained with trypan blue for differentiation of live/dead cells ($n = 3$). (B) Cell viability at select concentrations of PTX is shown in a bar graph (Error bars are SDs. $^*p < 0.05$, $^{***}p < 0.001$; Two-way ANOVA test followed by Bonferroni post hoc test).

at the concentrations used in the subsequent in vivo experiments (200 μg of UAN per mouse). The difference in cytotoxicity made by the presence of I domain on the surface of UAN was reexamined using the following PTX concentrations: 35, 1, and 0.2 μM (Fig. 3B). Although all other formulations were only marginally effective at PTX concentrations up to 35 μM, Id-UAN(PTX) was able to confer ~50% specific cell death at 1 μM.

### 3.4. Molecular interaction-guided tumor attenuation and systemic toxicity in vivo

After confirming selective delivery by the I domain, which targeted not only ICAM-1-positive tumor cells but also the stromal cells over-expressing ICAM-1, we evaluated the therapeutic efficacy of paclitaxel-loaded UAN particles in HeLa and 293T tumor xenografts. When the tumors reached a size of ~100 $mm^3$, mice were intravenously injected three times over 6 days with PBS, UAN(PTX), or Id-UAN(PTX). 3–4 days after the last injection, mice were sacrificed for further ex vivo analyses (Fig. 4A). Consistent with the tissue- and cellular-level biodistribution of UAN particles (Fig. 2), Id-UAN(PTX) treatment resulted in significant inhibition of tumor growth in both HeLa and 293T tumors (Fig. 4B), while little inhibition was observed in mice treated with UAN(PTX) compared to the PBS control (Fig. 4C). The image of the tumors recapitulated the notable difference between the efficacy of Id-UAN(PTX) and UAN(PTX) in tumor suppression (Fig. 4D). In addition to the difference in tumor size, the tumors treated with UAN(PTX) appeared darker due to abundant vasculatures in these tumors. On the other hand, tumors from mice administered with Id-UAN(PTX) seemed to lack the dark-red appearance, possibly due to the disruption of the tumor-associated vessels. Here, it needs to be reemphasized that the growth inhibition of 293T tumors by Id-UAN(PTX) should mainly come from the delivery of paclitaxel into the tumor stroma, presenting an evidence for tumor suppression achieved via drug carriers targeting the inflamed tumor microenvironment. To gauge the potential use of targeted UAN as drug carriers in clinics, we carried out a systemic toxicity assay associated with Id-UAN(PTX) by measuring the activity levels of ALT/AST enzymes in serum as well as the body weight of the mice (Fig. 4E and F). The ALT activity levels increased slightly 9–12 days after the first treatment but were below the levels indicative of liver toxicity (~56 mU/ml). Overall, no significant differences in ALT/AST levels and the rate of increase in body weight during the treatments were observed between the mice treated with UAN(PTX) and those treated with Id-UAN(PTX). Despite Id-UAN(PTX)'s cytotoxic effect on the tumors, the low to minimum levels of liver toxicity as well as the normal rate in body weight increase indicate that the particles were inert to non-specific interaction and were residing mostly in the extracellular space in the major organs.

## 4. Discussion

Utilizing polymeric nanoparticles as drug carriers, here we report that molecular markers induced in pro-inflammatory tumor microenvironment may provide a therapeutic strategy that is applicable to the suppression of different types of tumors independent of their tumor surface antigens. Among the surface markers that closely follow the degree of inflammation, we have chosen ICAM-1, a molecule that is rapidly upregulated in response to inflammation. With a targeting moiety against ICAM-1 incorporated into our nanoparticles, UAN was found to be internalized into not only ICAM-1-positive tumors but also the tumor-associated vasculature ($CD31^+$) and macrophages ($CD68^+$). The ability of ICAM-1-targeted nanoparticles to deliver paclitaxel into CD31/CD68-positive cells resulted in suppression of ICAM-1-negative 293T tumors.

Nanoparticle-based drug carriers that are devoid of molecular targeting rely heavily on leaky tumor vessels. However, tumor vessels available to many drug carriers of ~100 nm in size are sparsely distributed, particularly near high-level expression of vascular endothelial growth factor receptors [30]. Though non-leaky tumor microvasculature may still be permeable to molecules much smaller (less than ~12 nm), the large size of most drug carriers renders them inadequate for delivery in this route [31]. In order to address this problem, substantial research has been dedicated to identifying molecular markers in tumor-associated vasculature, also called the 'vascular zip codes' [10]. The luminal side of tumor-associated vessels is available to blood-borne

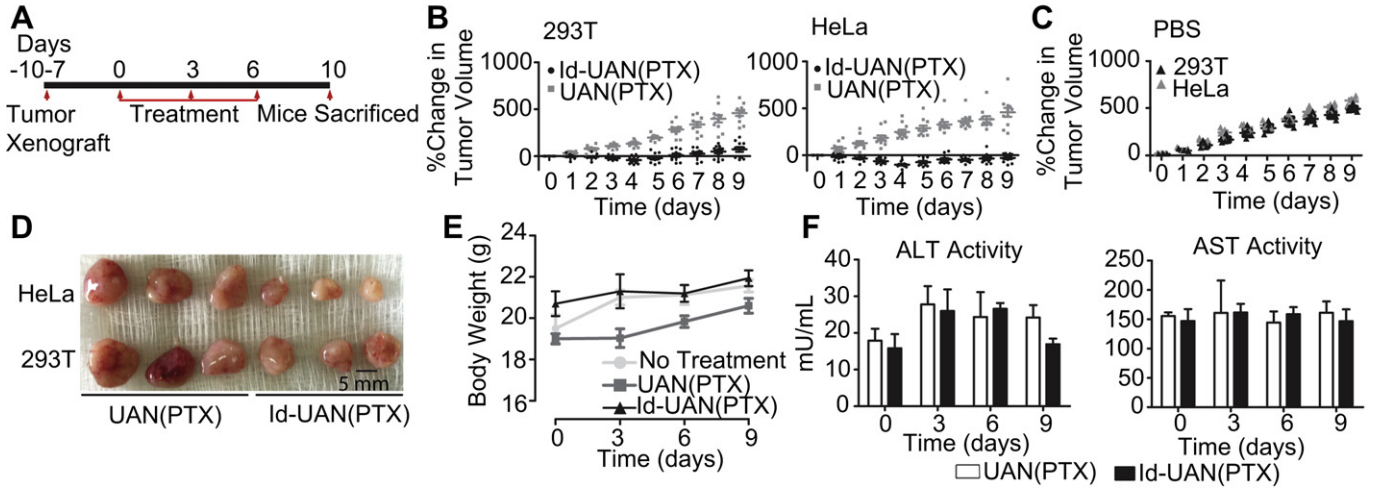


**Fig. 4.** Effects of Id-UAN(PTX) therapy on tumor growth in HeLa/293T xenografts and toxicity. (A) Timeline of tumor xenograft, nanoparticle injections, and ex vivo analysis is shown. (B) Mice bearing bilateral HeLa and 293T tumors were injected with either PBS, UAN(PTX), or Id-UAN(PTX). Tumor size in each mouse was measured daily. The difference in tumor size due to the treatment with Id-UAN(PTX) vs. UAN(PTX) was statistically significant beginning on day 3 for 293T and day 2 for HeLa ($p < 0.001$). (C) Change in tumor volume in mice receiving PBS. (D) Representative image of tumors excised from each group (scale bar, 5 mm). (E) Mean body weight of mice after each round of injections of UAN(PTX) or Id-UAN(PTX) on days 0, 3, 6, and 9. (F) Measurement of activity levels of ALT and AST in serum over the course of treatment. Blood was collected on days 0, 3, 6, and 9, prior to injection of nanoparticles (error bars are SDs).

particles and, once bound, the drug carriers can easily access the tumor interior [32]. Several molecules have been reported to be over- or uniquely expressed in tumor-associated vessels and used as therapy targets (e.g., $\alpha_v$ integrin [10,33,34]; ED-B domain of fibronectin [11], and VCAM-1 [35]). Recently, it has been demonstrated that VCAM-1, a cell adhesion molecule that interacts with $\alpha_4\beta_1$ integrin, was induced in the cerebral vasculature in the vicinity of brain metastases [35,36]. Similarly, we have found overexpression of ICAM-1 in the vascular endothelium associated with tumors [13,37–39]. Multimeric binding and clustering of ICAM-1 triggers cellular internalization of bound particles, and it has been shown that ICAM-1 can be recycled back to the cell surface after endocytosis [40], providing a mechanism to deliver drug agents in repeated doses. We have also found that ICAM-1 is induced in other tumor microenvironment mediators besides tumor-associated endothelium, such as macrophages and the tumors themselves [37,41–43]. Hence, using a targeting probe with tumor-homing properties for a molecular signature shared between tumor stroma and tumor cells can provide synergistic advantages.

The majority of drug carriers are designed to either induce non-specific cellular uptake or rapidly release drugs outside of cells after extravasation into or in the vicinity of tumors to achieve maximum therapeutic effect. However, nanoparticles possessing such properties would inevitably cause systemic toxicity as they would be prone to release cytotoxic drugs to phagocytic and parenchyma cells in major organs [2]. UAN nanoparticles used in this study were, however, designed to encapsulate and stably retain hydrophobic molecules. Without internalization into the cells, the release rate of cancer drugs from UAN would be too slow to produce significant cytotoxicity [28]. Polyethylene moiety forming the outer layer of UAN was introduced to greatly reduce opsonization and non-specific uptake by parenchyma and phagocytic cells. These properties of UAN nanoparticles in the absence of active targeting led to their accumulation mainly into interstitial space within the major organs, resulting in low levels of toxicity. The insignificant tumor attenuation by the non-targeted UAN is also ascribed to the need for a much higher dose of PTX required to have cytotoxic effects compared to that of ICAM-1-selective delivery ($EC_{50} = 1$ μM with targeted vs. 37.5 μM with non-targeted). The nickel-NTA moiety present at the terminal hydroxyl group of polyethylene makes UAN particles highly versatile for facile conjugation with targeting ligands with a His-tag, obviating highly unpredictable chemical conjugations. The ability of drug carriers to actively bind target cells is vital to lessen the barriers created by the elevated interstitial fluid pressure [38,44,45], which retards the penetration of drug carriers deep into tumors and even forces them back into circulation. Rapid binding and subsequent receptor-mediated endocytosis, therefore, may overcome such limitations of many non-targeted drug carriers.

## 5. Conclusions

In this work, we have successfully engineered polymeric drug carriers to target ICAM-1-expressing tumors as well as inflamed tumor microenvironment. UAN has exhibited its advantages as a targeted drug carrier for its ability to evade the mononuclear phagocytic system and cause low levels of systemic toxicity. By targeting an inflammatory marker in tumor vessels, Id-UAN particles may act as a double-edged sword: Not only will they be able to localize drug delivery to the tumor site, they may also inhibit the infiltration of LFA-1-expressing pro-tumor immune cells by occupying ICAM-1 on endothelium or by promoting internalization of the receptors. As demonstrated with ICAM-1-negative 293T tumor, the upregulation of ICAM-1 in the tumor environment can be utilized to deliver chemotherapeutics to tumors lacking unique markers. UAN's ability to encapsulate and deliver a cocktail of hydrophobic drugs may also aid in addressing the problems of drug-resistance.

## Acknowledgments

This work was funded by a National Science Foundation (NSF) GK-12 Fellowship Award and Business for International Cooperative R&D between Industry, Academy, and Research Institute (Korea Small and Medium Business Administration, Grant No. 00042115).

## References

[1] Yuan F, Dellian M, Fukumura D, Leunig M, Berk DA, Torchilin VP, et al. Vascular permeability in a human tumor xenograft: molecular size dependence and cutoff size. Cancer Res 1995;55:3752–6.
[2] Li SD, Huang L. Pharmacokinetics and biodistribution of nanoparticles. Mol Pharm 2008;5:496–504.
[3] Hambley TW, Hait WN. Is anticancer drug development heading in the right direction? Cancer Res 2009;69:1259–62.
[4] Jain RK. Transport of molecules, particles, and cells in solid tumors. Annu Rev Biomed Eng 1999;1:241–63.
[5] Danquah MK, Zhang XA, Mahato RI. Extravasation of polymeric nanomedicines across tumor vasculature. Adv Drug Deliv Rev 2011;63:623–39.
[6] Jain RK, Stylianopoulos T. Delivering nanomedicine to solid tumors. Nat Rev Clin Oncol 2010;7:653–64.
[7] Kong G, Braun RD, Dewhirst MW. Hyperthermia enables tumor-specific nanoparticle delivery: effect of particle size. Cancer Res 2000;60:4440–5.
[8] Chen B, Pogue BW, Luna JM, Hardman RL, Hoopes PJ, Hasan T. Tumor vascular permeabilization by vascular-targeting photosensitization: effects, mechanism, and therapeutic implications. Clin Cancer Res 2006;12:917–23.
[9] Watson KD, Lai CY, Qin S, Kruse DE, Lin YC, Seo JW, et al. Ultrasound increases nanoparticle delivery by reducing intratumoral pressure and increasing transport in epithelial and epithelial-mesenchymal transition tumors. Cancer Res 2012;72:1485–93.
[10] Sugahara KN, Teesalu T, Karmali PP, Kotamraju VR, Agemy L, Girard OM, et al. Tissue-penetrating delivery of compounds and nanoparticles into tumors. Cancer Cell 2009;16:510–20.
[11] Nilsson F, Kosmehl H, Zardi L, Neri D. Targeted delivery of tissue factor to the ED-B domain of fibronectin, a marker of angiogenesis, mediates the infarction of solid tumors in mice. Cancer Res 2001;61:711–6.
[12] Turk MJ, Waters DJ, Low PS. Folate-conjugated liposomes preferentially target macrophages associated with ovarian carcinoma. Cancer Lett 2004;213:165–72.
[13] Chen X, Wong R, Khalidov I, Wang AY, Leelawattanachai J, Wang Y, et al. Inflamed leukocyte-mimetic nanoparticles for molecular imaging of inflammation. Biomaterials 2011;32:7651–61.
[14] Coussens LM, Werb Z. Inflammation and cancer. Nature 2002;420:860–7.
[15] Grivennikov SI, Greten FR, Karin M. Immunity, inflammation, and cancer. Cell 2010;140:883–99.
[16] Ogawa Y, Hirakawa K, Nakata B, Fujihara T, Sawada T, Kato Y, et al. Expression of intercellular adhesion molecule-1 in invasive breast cancer reflects low growth potential, negative lymph node involvement, and good prognosis. Clin Cancer Res 1998;4:31–6.
[17] Kelly CP, O'Keane JC, Orellana J, Schroy 3rd PC, Yang S, LaMont JT, et al. Human colon cancer cells express ICAM-1 in vivo and support LFA-1-dependent lymphocyte adhesion in vitro. Am J Physiol 1992;263:G864–70.
[18] Passlick B, Izbicki JR, Simmel S, Kubuschok B, Karg O, Habekost M, et al. Expression of major histocompatibility class I and class II antigens and intercellular adhesion molecule-1 on operable non-small cell lung carcinomas: frequency and prognostic significance. Eur J Cancer 1994;30A:376–81.
[19] Tomita Y, Nishiyama T, Watanabe H, Fujiwara M, Sato S. Expression of intercellular adhesion molecule-1 (ICAM-1) on renal-cell cancer: possible significance in host immune responses. Int J Cancer 1990;46:1001–6.
[20] Koyama S, Ebihara T, Fukao K. Expression of intercellular adhesion molecule 1 (ICAM-1) during the development of invasion and/or metastasis of gastric carcinoma. J Cancer Res Clin Oncol 1992;118:609–14.
[21] Shimoyama S, Gansauge F, Gansauge S, Widmaier U, Oohara T, Beger HG. Overexpression of intercellular adhesion molecule-1 (ICAM-1) in pancreatic adenocarcinoma in comparison with normal pancreas. Pancreas 1997;14:181–6.
[22] Buitrago D, Keutgen XM, Crowley M, Filicori F, Aldailami H, Hoda R, et al. Intercellular adhesion molecule-1 (ICAM-1) is upregulated in aggressive papillary thyroid carcinoma. Ann Surg Oncol 2012;19:973–80.
[23] Schroder C, Witzel I, Muller V, Krenkel S, Wirtz RM, Janicke F, et al. Prognostic value of intercellular adhesion molecule (ICAM)-1 expression in breast cancer. J Cancer Res Clin Oncol 2011;137:1193–201.

[24] Roland CL, Dineen SP, Toombs JE, Carbon JG, Smith CW, Brekken RA, et al. Tumor-derived intercellular adhesion molecule-1 mediates tumor-associated leukocyte infiltration in orthotopic pancreatic xenografts. Exp Biol Med (Maywood) 2010;235:263–70.
[25] Shimaoka M, Xiao T, Liu JH, Yang Y, Dong Y, Jun CD, et al. Structures of the alpha L I domain and its complex with ICAM-1 reveal a shape-shifting pathway for integrin regulation. Cell 2003;112:99–111.
[26] Jin M, Song G, Carman CV, Kim YS, Astrof NS, Shimaoka M, et al. Directed evolution to probe protein allostery and integrin I domains of 200,000-fold higher affinity. Proc Natl Acad Sci U S A 2006;103:5758–63.
[27] Kang S, Park T, Chen X, Dickens G, Lee B, Lu K, et al. Tunable physiologic interactions of adhesion molecules for inflamed cell-selective drug delivery. Biomaterials 2011;32:3487–98.
[28] Park S, Kang S, Veach AJ, Vedvyas Y, Zarnegar R, Kim JY, et al. Self-assembled nanoplatform for targeted delivery of chemotherapy agents via affinity-regulated molecular interactions. Biomaterials 2010;31:7766–75.
[29] Wong R, Chen X, Wang Y, Hu X, Jin MM. Visualizing and quantifying acute inflammation using ICAM-1 specific nanoparticles and MRI quantitative susceptibility mapping. Ann Biomed Eng 2011;40:1328–38.
[30] Karathanasis E, Chan L, Karumbaiah L, McNeeley K, D'Orsi CJ, Annapragada AV, et al. Tumor vascular permeability to a nanoprobe correlates to tumor-specific expression levels of angiogenic markers. PLoS One 2009;4:e5843.
[31] Sarin H, Kanevsky AS, Wu H, Sousa AA, Wilson CM, Aronova MA, et al. Physiologic upper limit of pore size in the blood-tumor barrier of malignant solid tumors. J Transl Med 2009;7:51.
[32] Ruoslahti E, Bhatia SN, Sailor MJ. Targeting of drugs and nanoparticles to tumors. J Cell Biol 2010;188:759–68.
[33] Hood JD, Bednarski M, Frausto R, Guccione S, Reisfeld RA, Xiang R, et al. Tumor regression by targeted gene delivery to the neovasculature. Science 2002;296:2404–7.
[34] Murphy EA, Majeti BK, Barnes LA, Makale M, Weis SM, Lutu-Fuga K, et al. Nanoparticle-mediated drug delivery to tumor vasculature suppresses metastasis. Proc Natl Acad Sci USA 2008;105:9343–8.
[35] Serres S, Soto MS, Hamilton A, McAteer MA, Carbonell WS, Robson MD, et al. Molecular MRI enables early and sensitive detection of brain metastases. Proc Natl Acad Sci USA 2012;109:6674–9.
[36] Dienst A, Grunow A, Unruh M, Rabausch B, Nor JE, Fries JW, et al. Specific occlusion of murine and human tumor vasculature by VCAM-1-targeted recombinant fusion proteins. J Natl Cancer Inst 2005;97:733–47.
[37] Melder RJ, Koenig GC, Witwer BP, Safabakhsh N, Munn LL, Jain RK. During angiogenesis, vascular endothelial growth factor and basic fibroblast growth factor regulate natural killer cell adhesion to tumor endothelium. Nat Med 1996;2:992–7.
[38] Fukumura D, Jain RK. Tumor microvasculature and microenvironment: targets for anti-angiogenesis and normalization. Microvasc Res 2007;74:72–84.
[39] Yoong KF, McNab G, Hubscher SG, Adams DH. Vascular adhesion protein-1 and ICAM-1 support the adhesion of tumor-infiltrating lymphocytes to tumor endothelium in human hepatocellular carcinoma. J Immunol 1998;160:3978–88.
[40] Muro S, Gajewski C, Koval M, Muzykantov VR. ICAM-1 recycling in endothelial cells: a novel pathway for sustained intracellular delivery and prolonged effects of drugs. Blood 2005;105:650–8.
[41] Mizoi T, Ohtani H, Suzuki Y, Shiiba K, Matsuno S, Nagura H. Intercellular adhesion molecule-1 expression by macrophages in human gastrointestinal carcinoma: possible roles as host immune/inflammatory reaction. Pathol Int 1995;45:565–72.
[42] Blank C, Brown I, Kacha AK, Markiewicz MA, Gajewski TF. ICAM-1 contributes to but is not essential for tumor antigen cross-priming and $CD8^+$ T cell-mediated tumor rejection in vivo. J Immunol 2005;174:3416–20.
[43] Fukumura D, Kashiwagi S, Jain RK. The role of nitric oxide in tumour progression. Nat Rev Cancer 2006;6:521–34.
[44] Heldin CH, Rubin K, Pietras K, Ostman A. High interstitial fluid pressure – an obstacle in cancer therapy. Nat Rev Cancer 2004;4:806–13.
[45] Padera TP, Kadambi A, di Tomaso E, Carreira CM, Brown EB, Boucher Y, et al. Lymphatic metastasis in the absence of functional intratumor lymphatics. Science 2002;296:1883–6.